instruments

MDPI

Article

High Harmonic Generation Seeding Echo-Enabled Harmonic Generation toward a Storage Ring-Based Tender and Hard X-ray-Free Electron Laser

Xi Yang *, Lihua Yu, Victor Smaluk and Timur Shaftan

National Synchrotron Light Source II, Brookhaven National Laboratory, Upton, NY 11973, USA; lhyu@bnl.gov (L.Y.); vsmalyuk@bnl.gov (V.S.); shaftan@bnl.gov (T.S.)
* Correspondence: xiyang@bnl.gov

Abstract: To align with the global trend of integrating synchrotron light source (SLS) and free electron laser (FEL) facilities on one site, in line with examples such as SPring-8 and SACLA in Japan and ELETTRA and FERMI in Italy, we actively explore FEL options leveraging the ultralow-emittance electron beam of the NSLS-II upgrade. These options show promising potential for synergy with storage ring (SR) operations, thereby significantly enhancing our facility's capabilities. Echo-enabled harmonic generation (EEHG) is well-suited to SR-based FELs, and has already been demonstrated with the capability of generating extremely narrow bandwidth as well as high brightness, realized using diffraction-limited short pulses in transverse planes and Fourier transform-limited bandwidth in the soft X-ray spectrum. However, regarding a conventional EEHG scheme, the combination of the shortest seed laser wavelength (256 nm) and highest harmonic (200) sets the short wavelength limit to λ = 1.28 nm. To further extend the short wavelength limit down to the tender and hard X-ray region, a vital option is to shorten the seed laser wavelength. Thanks to recent advances in high harmonic generation (HHG), packing 10^9 photons at one harmonic within a few-femtosecond pulse could turn such a novel HHG source into an ideal seeding for EEHG. Thus, compared to the cascaded EEHG, the HHG seeding option could not only lower the cost, but also free the SR space for accommodating more user beamlines. Moreover, to mitigate the SASE background noise on the sample and detector, we combine the HHG seeding EEHG with the crab cavity short pulse scheme for maximum benefit.

Keywords: storage ring-based free electron laser; echo-enabled harmonic generation; high harmonic generation source; synchrotron light source; laser seeding

Citation: Yang, X.; Yu, L.; Smaluk, V.; Shaftan, T. High Harmonic Generation Seeding Echo-Enabled Harmonic Generation toward a Storage Ring-Based Tender and Hard X-ray-Free Electron Laser. *Instruments* **2024**, *8*, 35. https://doi.org/10.3390/instruments8020035

Academic Editor: Antonio Ereditato

Received: 16 April 2024
Revised: 27 May 2024
Accepted: 31 May 2024
Published: 2 June 2024

1. Introduction

The synchrotron light source (SLS) is a major tool for a wide range of scientific endeavors, in particular because of the high pulse repetition rate it enables. To expand the capabilities of future fourth-generation diffraction-limited (DL) SLSs, storage ring (SR)-based FELs could constitute invaluable tools in exploring nature at the ultrasmall spatial and ultrafast temporal scales. Compared to linac sources, SLS has a few key constraints: long bunch length (at least a few picoseconds), large energy spread (in the order of 10^{-3}), and low peak current (<300 A). Because of those limitations, some form of external seeding from a laser system is required to generate shorter coherent radiation (CR) pulses, before one can take the full advantages of the ultra-stable (orbit motion in the level of a micrometer) and diffraction-limited (10 s picometer emittance) electron beam at a high repetition rate ($\geq$1 kHz). Echo-enabled harmonic generation (EEHG) is well-suited to SR-based FELs (less sensitive to energy spread, and no need of any lattice change) compared to High Gain Harmonic Generation (HGHG) and Angular Dispersion Enhanced Prebunching [1–12]. Moreover, for the EEHG approach, the maximal bunching (b_n) can be achieved with the energy modulation much smaller than $n\sigma_E$ as required for the HGHG case, where n is the harmonic and σ_E is the energy spread. From harmonic 50 to harmonic 200, only about

30–40% decrease in the achievable bunching factor is predicted while using a reasonable laser power for seeding. Regarding the nominal seeding via a conventional solid-state laser system, e.g., the third harmonic of Ti:sapphire laser at the wavelength of 256 nm [1–3,13], the shortest wavelength that can be achieved is determined by the combination of the short seed laser wavelength of 256 nm and the highest harmonic of 200, which is difficult to achieve, around $\lambda = 256\ \text{nm}/200 = 1.28\ \text{nm}$ [14].

2. Results

2.1. SR-Based EEHG FEL Seeded with High Harmonic Generation

To extend the short wavelength limit down to the tender and hard X-ray region, straightforward approaches are to increase the high harmonic above 200 and/or utilize a seed laser with the wavelength less than 256 nm. Regarding the first option, there exist some obstacles (e.g., the required energy modulation being too large and de-bunching being too fast), which prevent the high harmonic from exceeding 200. Thus, finding a way to shorten the seed laser wavelength becomes the most feasible option. One way is to apply the cascaded EEHG scheme [13], as shown in Figure 1a, and the other is to find a seeding source with a short wavelength [10–12], as shown in Figure 1b. The drawbacks of the cascade scheme are not only significantly scaling up the occupancy of an SR, which is already crowded, as well as the overall cost, but also increasing the technical challenges and the operational complexities. Thanks to the rapid advance of the high harmonic generation (HHG) in the spectrum region of extreme ultraviolet (EUV) and soft X-ray in the last decade [10–12], the capability of packing more than 10^9 photons within a few femtosecond pulse duration and 10^{-3} spectrum width at a repetition rate exceeding 5 kHz could turn such a novel HHG source into an ideal seed (Figure 2) for the generation of CR in the X-ray wavelengths via a conventional EEHG approach [15–25]. To mitigate the detrimental fluctuations affecting the final EEHG bunching outcome, we choose to operate optimally rather than overdriven during the HHG process. This reduces fluctuations to less than 5%, albeit resulting in fewer photons per pulse (10^9 photons per pulse). An EUV HHG source seeding EEHG scheme could enable a compact design of the SR-based FEL toward the tender and hard X-ray region, eliminating the need of building two cascaded EEHG beamlines [13]. Considering the intrinsic features of the EEHG—forming multiple energy stripes in the longitudinal phase space (LPS) via the first-stage pre-bunching then utilizing an HGHG type of harmonic bunching in the second stage [13]—it would be ideal if one can seed the second stage with an optimized EUV-HHG source at the shortest possible wavelength 28.5 nm, whereas the highest peak power, a few-femtosecond pulse duration and narrowest linewidth of 0.1–0.2 eV are simultaneously fulfilled. These HHG parameters, including $1{\cdot}10^9$ photons per pulse, are derived from an overall photon flux of $6{\cdot}10^{12}$ photons per second at a repetition rate of 5 kHz. They can be achieved under optimally driven conditions, a capability provided by KMLabs Inc., founded by Dr. Henry C. Kapteyn [26]. In addition, to optimize the energy-stripe formation in the LPS for maximum prebunching under the peak power constraint of an EUV-HHG source, limited by $1{\cdot}10^9$ photons per pulse with a 10 fs pulse duration, it is preferrable to seed the first stage with a conventional Ti:sapphire laser at its third harmonic (256 nm) and vary the two-stage separation to optimize the momentum compaction of the first stage (R_1) [1–3], while simultaneously mitigating the smearing effect induced with incoherent synchrotron radiation (ISR) [13]. The optical transport lines for the 256 nm seed laser of stage 1 and the EUV-HHG source of stage 2 should be built in an ultra-high vacuum to avoid air turbulence, achieving the required *μrad*-level spatial pointing jitter, which is limited by the transverse walk-off between the seed laser and the electron bunch, not exceeding a small fraction of the beam size [13]. As the result, one can achieve the shortest wavelength of λ = 0.34 nm. See Table 1 for details.

Table 1. Summary of three EEHG options: conventional (named single beamline), novel seeding via EUV HHG source (named HHG seeded EEHG), and cascaded EEHG. It includes the wavelengths of seed laser 1 and 2 and CR output, the estimated costs, the number of photons per pulse and per second, the spectrum bandwidth, the coherent length, the pulse duration, the spectral tunability, the repetition rate, and the output power in average, regarding those three options for the NSLS-II upgrade lattice. By varying the HHG pump laser wavelength (e.g., Yb 1030 nm and Ti:sapphire 800 nm) and gas type (Xenon, Krypton, and Argon) [10–12], the maximum wavelength in the HHG seeded EEHG case can extend up to >1 nm, almost overlapping with the single-beamline EEHG. The estimated cost does not include the portion of short-pulse crab cavity scheme.

EEHG	λ_{1seed}	λ_{2seed}	$\lambda_{r,min}$	E_{ph}	Cost	Photon per Pulse	Photon/s	Spectral Width	Coherent Length	Pulse Width in FWHM	Spectral Tunability	Repetition Rate	Output Power in Average
	nm	nm	nm	eV	$				m	s	nm	kHz	W
single-beamline	256	256	1.28	973	1000 k	2.00×10^{10}	2.00×10^{14}	4.30×10^{-6}	1.28×10^{-4}	1.00×10^{-12}	1.25–50	1.00×10^{1}	3.00×10^{-2}
HHG seeded	256	28.49	1.016	1219	1300 k	1.02×10^{10}	5.11×10^{13}	1.03×10^{-3}	1.28×10^{-7}	3.00×10^{-15}	0.341–1.016	5.00×10^{0}	9.97×10^{-3}
EEHG	256	28.49	0.341	3627	1300 k	1.44×10^{9}	7.18×10^{12}	3.46×10^{-4}	1.28×10^{-7}	3.00×10^{-15}		5.00×10^{0}	4.16×10^{-3}
Cascaded EEHG	256	12.8	0.128	9727	2000 k	1.10×10^{8}	1.10×10^{11}	4.30×10^{-7}	1.28×10^{-4}	1.00×10^{-12}	0.125–0.5	1.00×10^{0}	2.00×10^{-4}

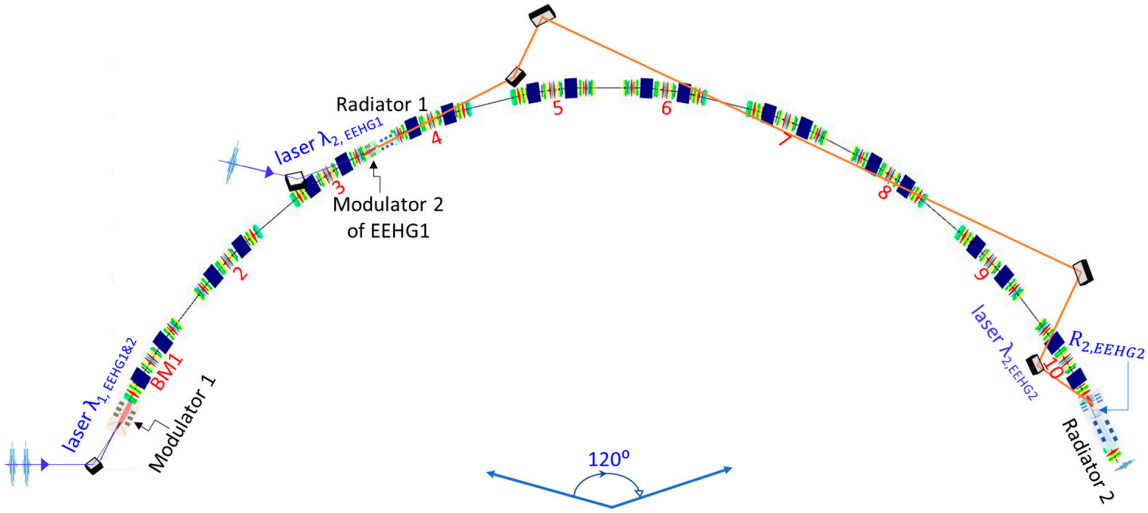

(**a**)

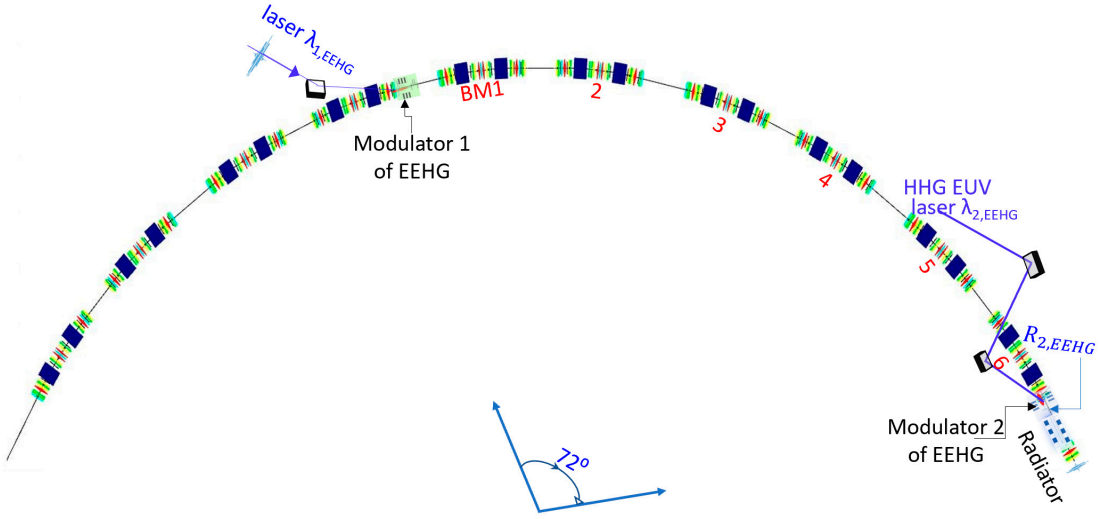

(**b**)

Figure 1. (**a**) Layout of the cascaded EEHG. (**b**) Layout of the EEHG seeded with an HHG source for the second stage. Here, BM represents the bending magnets between two straights. The numbers start from the first BM right after the stage-1 modulator.

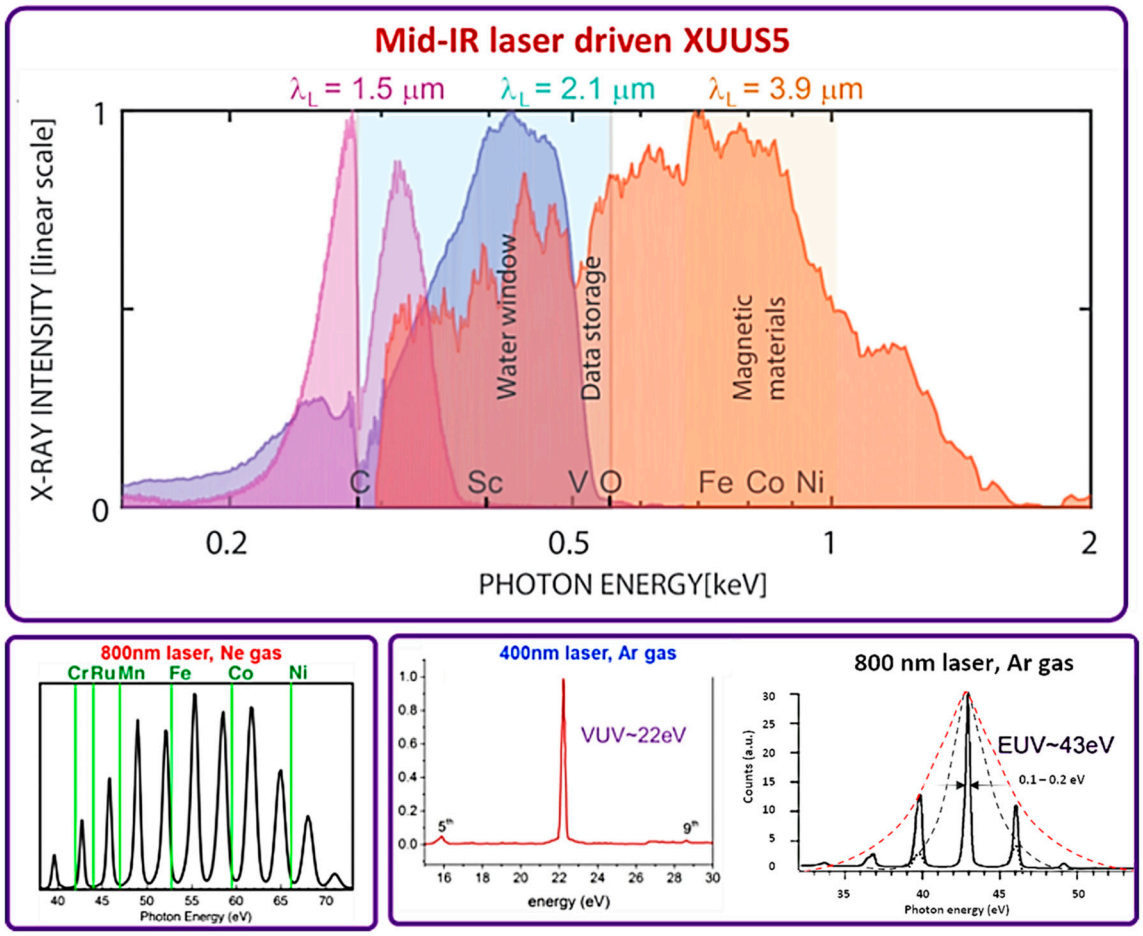

Figure 2. HHG EUV source spectrum [26]. At the chosen harmonic, the HHG source can be optimized to suppress the neighboring harmonics (indicated by the change of the envelope from the red dashed line to the black dashed line in the bottom right plot). In total, $1{\cdot}10^9$ photons per pulse are derived from $6{\cdot}10^{12}$ (optimally driven) photons/s at the repetition rate of 5 kHz [26].

The reason why we choose an HHG source as the seed for the second stage of the EEHG while still keeping the third harmonic of a Ti:sapphire laser with the wavelength of 256 nm as the seed for the first stage (Figure 1b) is because: (1) the ultimate bunching factor is mainly determined by the energy modulation of the first stage relative to the energy spread (denoted A_1), thus, the required power of seed laser 1 can be quite high and likely needs to achieve an A_1 substantially greater than one (only Ti:sapphire can meet those requirements); and (2) the energy modulation of the second stage is quite similar to the HGHG [27–30] in the sense that they both require fine tuning to maximize the bunching factor regarding a specific harmonic.

However, the HHG laser pulse is very short, only a few femtoseconds, compared to the 20 picosecond electron, and the corresponding self-amplified spontaneous emission (SASE) background noise, akin to the conventional synchrotron background, can be problematic as it accumulates across the entire electron bunch. Hence, one must carefully examine the enhancement factor, which is defined as the ratio of the signal from pre-bunched electron portion coherently radiating and the noise obtained by integrating the SASE background across the entire electron bunch. The following issues need to be addressed and well understood:

(1) The effective peak power of an HHG pulse P_{HHG} can be calculated via the following equation:

$$P_{HHG} = N_1 \cdot E_{ph} / \delta_{t,FWHM}. \quad (1)$$

It equals the number of photons per pulse, N_1, timing photon energy, E_{ph}, then being divided by the temporal pulse duration in FWHM $\delta_{t,FWHM}$.

(2) The transmission efficiency of an EUV pulse from the HHG source point to the second stage seeding position in the EEHG setup ($\eta_{transmission}$) can be estimated as:

$$\eta_{transmission} = T \cdot \eta_{trans,\ mod}. \quad (2)$$

The total reflectivity of two EUV mirrors at the HHG seed wavelength equals to $T = R^2$, around 30% [13]. In an overly optimistic case, one could directly send an HHG pulse into the modulator, with T being closer to 100%. The transverse matching between the seed laser and the FEL mode profiles determines the overlapping efficiency, which could be optimized with $\eta_{trans,\ mod}$ close to 100%. The HHG source can be focused down to a few microns [26], which is close to the electron beam size in modulator 2. The longitudinal laser-electron overlap could be achieved by tuning the laser timing, as an example, using a vector modulator, while observing laser and undulator pulses with a streak camera. The transverse overlap could be controlled with motorized laser mirrors at the optical transport line. A primary indication of successful laser–electron interaction could be the coherent emission observed at a dedicated dipole beamline with a Schottky diode [31]. This phenomenon arises from the energy-modulated electrons forming sub-picosecond current spikes in the longitudinal charge distribution, thereby generating broadband THz radiation similar to equally short bunches. As an example, while the FLASH setup was constrained by existing configurations, due to space restrictions of the facility, the HHG source was located below the laboratory floor level, thus, its optical transport line utilized more mirrors (totaling six) than necessary, resulting in a significant loss of around 95% [32,33]. In contrast, we are currently in the early stage of conceptual design. This allows us the opportunity to optimize the transport line optics with fewer mirrors, while still ensuring effective overlap between the seed laser and electron beam. Consequently, we anticipate a much higher transfer efficiency compared to the HHG seeding case at the FLASH facility. Furthermore, by shortening the period, and consequently the length, of modulator 2 (see details of modulator-2 parameters later in this section), we can mitigate the impact of HHG source divergence. The overall transmission efficiency $\eta_{transmission}$, which is the product of the total reflectivity and overlapping efficiency, are assumed to be close to 100%. It is highly possible that with the future progress on the peak power and bandwidth of the HHG source, the stringent requirement of $\eta_{transmission}$ could be further relaxed and well fulfilled.

(3) The spectrum also limits the fraction of photons per HHG pulse that can be used for seeding the second stage, adding another factor, η_{SBW}. This quantity may be large, since it is possible to optimize the HHG source to have the majority of the pulse energy in a small number of harmonics. We do not take the neighboring harmonics into account, although they might still be useful for the modulation if the modulator is sufficiently short. Thus, it is possible to have the following [26]:

$$\eta_{SBW} \approx 1. \quad (3)$$

(4) Combining these effects, the available power in the EUV for modulating the beam is the following:

$$P_{avail} = P_{HHG} \cdot \eta_{SBW} \cdot \eta_{transmission}. \quad (4)$$

Shown as the red curve in Figure 3, this quantity must exceed the required seed laser-2 power (black curve) predicted using the EEHG optimizer, a tool implemented in our early studies [1], with the optimized stage-1 energy modulation and momentum compaction of chicane-1, which are fixed to A_1 = 2.5 and R_1 = 8.4 mm (two-stage separation of six cells) [2,3,13]. All the bunched structures in the electron beam are completely washed out within one turn due to its corresponding momentum compaction. For example, in the NSLS-II upgrade, this corresponds to 42 mm (30 cells × 1.4 mm/cell). The only difference when this bunch circulates around the ring and returns to the stage-1 modulator is the increased energy spread for the modulated beam slice. One can choose either to wait for a

radiation damping time (e.g., about 20 ms for APS-Upgrade lattice [2]) for the increased energy spread to damp down to the equilibrium value or to select a different part of this electron bunch or a different electron bunch for seeding [1–3]. The intersection of those two curves determines the shortest wavelength limit of 0.34 nm and photon energy 3.6 keV.

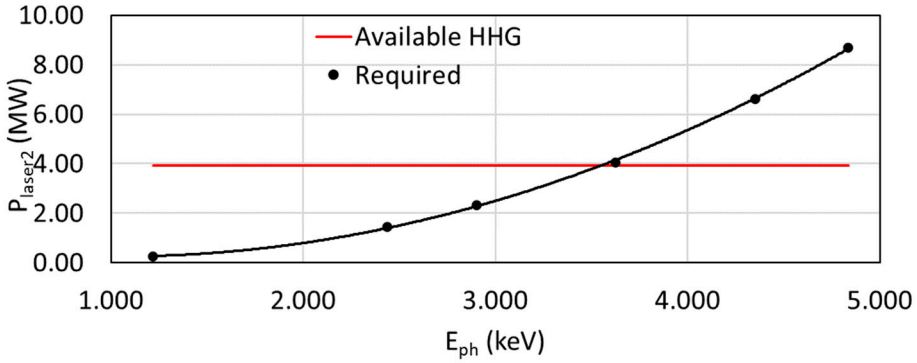

Figure 3. Considering an HHG source at the wavelength of 28.5 nm being applied to seed the second stage of the EEHG, the available and required seed laser powers are plotted as red and black curves, respectively. Here, the available seed laser power is estimated by multiplying the peak power of the HHG source with the seeding efficiency in the spectrum domain and the transmission efficiency from the source to the second stage modulator (Equation (4)). The required seed laser-2 power is estimated via the EEHG optimizer with the optimized stage-1 energy modulation and momentum compaction of chicane-1 being fixed to A_1 = 2.5 and R_1 = 8.4 mm, respectively.

(5) The final pre-bunched electron beam produced using the EEHG seeding scheme radiates coherently from the entire modulated beam slice. The CR power initially scales quadratically with the bunching factor and can be estimated as:

$$P_{CR} = 1.6 \cdot \left(\frac{1}{4\pi\gamma}\right)^3 \left[\frac{2\pi^2}{\Sigma_b}(f_b(\xi)\lambda_u K_u)^2 \frac{I_{peak}}{I_A}\right] \cdot |b_n|^2 \cdot P_{beam} \cdot \left(\frac{4\pi\sqrt{3}\cdot Z}{\lambda_u}\right)^2. \quad (5)$$

where $\Sigma_b = 2\pi\sigma_x\sigma_y$ is the electron beam cross-section, λ_u is the undulator period, I_{peak} is the electron beam peak current, $I_A = e_0 c/r_0 \sim 17\,kA$ is the Alfvén current (being e_0 the electron charge and r_0 the electron classical radius), $K_u = B_0[\mathrm{kG}]\lambda_u[\mathrm{cm}]/10.71$ is the dimensionless undulator parameter, and b_n is the bunching factor (see later for details) [13,25]. The function $f_b(\xi) = J_0(\xi) - J_1(\xi)$, where $\xi = K_u^2/(4+2K_u^2)$ is a kinematic coupling factor accounting for the average phase mismatch in linear undulators. $P_{beam} = m_0c^2\gamma I_{peak}/e_0$ is the peak power carrier by the electron beam with relativistic factor γ. Equation (5) is only valid for the distance Z, over which the bunching retains its value and the radiation slippage is shorter than the length of the pre-bunched region. Note that FEL gain is negligible.

(6) Incoherent (SASE) background noise is contributed by the portion of the spectrum from the white noise of the entire electron bunch overlapping with the FEL gain bandwidth (GBW) (Equation (6) [13,25].

$$P_{inc} = \alpha \cdot \left(\frac{1}{4\pi\gamma}\right)^3 \left[\frac{2\pi^2}{\Sigma_b}(f_b(\xi)\lambda_u K_u)^2 \frac{I_{peak}}{I_A}\right] \cdot \frac{c\cdot E_0}{\lambda} \cdot \frac{4\pi\sqrt{3}\cdot Z}{\lambda_u} \quad (6)$$

Here, $\alpha = \frac{1}{9}4\pi\sqrt{3} \approx 2.42$, and c and E_0 are the speed of light and the electron beam energy, respectively. FEL gain is also negligible for the incoherent radiation.

(7) The ratio of the CR signal over the SASE background noise R_{obs} (namely, the factor of CR exceeding SASE) can be estimated via Equation (7):

$$R_{obs} = P_{CR}/P_{inc} \cdot \sigma_{t,\,CR}/\sigma_{t,beam}. \quad (7)$$

The great challenge here is to maximize the pre-bunching by allowing the final energy spread to increase since the CR power is quadratically proportional to the pre-bunching factor (Equation (4) with a fixed radiator length as short as a few meters. Based on our earlier studies, the optimal bunching factor strongly depends on the allowable radiator length [1–3]; we apply a similar strategy to the current design. In this manuscript, we limit our design to the NSLS-II upgrade lattice with the radiator length of 3 m. The only exception could be a large-sized storage ring, e.g., Petra IV and a similar DL-SLS in the PEP tunnel (named SDLS) [34,35]; the insertion device (ID) section can be as long as tens meters. The pulse duration of an HHG source is often limited to less than 10 femtoseconds; regarding the EUV wavelength required by seeding, the pulse duration is currently limited to a few femtoseconds, as shown in Figure 2. Compared to a 20 picosecond electron bunch, the SASE background noise can be quite significant. To make the CR signal exceed the SASE background noise, one must maximize the initial pre-bunching, as shown in Figure 4a. With the constraint of the peak power of an HHG source, shown as the red curve in Figure 3, one must maximize the bunching factor via varying the modulator parameters as well as increasing the energy modulation. The total energy spread and the momentum compaction of chicane 2 are shown as Figures 4b and 4c, respectively. The initial bunching factor is significantly higher, as shown in Figure 4a, ranging from 7% to 10%. In conjunction with the minimized beta functions (1.7 m) and emittances (25 pm in x and 5 pm in y) in the radiator, one can achieve the CR peak power as high as a few giga-watt (GW), as shown in Figure 4d. As a result, the CR signal surpasses the SASE background noise (black curve in Figure 5a) by a factor ranging from 1.2 up to 7.1. Such an enhancement should be observable by any beamline detector. Furthermore, if one applies the gating technique, the enhancement factor can be further improved by several orders of magnitude, closer to the ratio of the peak power of the CR pulse and the SASE background noise. However, commercially available gating techniques are quite limited, e.g., exceeding 1 ps, still, the sample is exposed to the SASE background from the entire electron bunch. Thus, to mitigate the SASE background striking the detector as well as the sample, the crab cavity short pulse scheme is much more preferrable (see Section 2 in Results).

We chose modulator 2 with a short period of 5 cm and the length of 1.5 m, and stage-1 energy modulation of $A_1 = 2.5$ instead of $A_1 = 1.3$ compared to the cascaded scheme [13]. Especially, A_2 is optimized ranging from 0.2 to 0.6, requiring much less power of the HHG seed as well as contributing much less heating effect to the beam energy spread compared to stage 1.

This ultimate short wavelength limit $\lambda = 0.34$ nm is only a factor of three longer than the one set by the cascaded EEHG scheme. Moreover, the hardware required by the HHG seeding EEHG scheme is quite similar to what is needed by a conventional EEHG, and it is much less than what is needed by the cascaded EEHG. This could reduce the total cost down to nearly half of the cascaded case; see Table 1 for details. Furthermore, there is no need of the optical transport line, which is used to transfer the output of the CR pulse from the first EEHG beamline as the input seed to the second modulator of the second EEHG beamline, greatly mitigating the technical challenges and allowing for more spaces for building user beamlines. The performances of the cascaded and HHG seeding options are quite similar, except that the HHG seeding generates a CR pulse with the duration of a few femtoseconds, which is limited by the HHG seed pulse length; instead, a few picoseconds is needed for the cascaded case. In addition, the HHG pulse is modified by both the mirror and the modulator. The pulse length should be at least the number of undulator periods times the seed wavelength 28.5 nm, which corresponds to ~3 fs. To take full advantage of the ultrafast HHG seeding EEHG scheme, one could potentially split the drive laser pulse into two branches: one for the HHG production, and the other being transmitted to the experimental hutch for pump-probe experiments. Thus, the CR pulse from the radiator and the laser pulse would be perfectly synchronized with the timing jitter in the femtosecond level. Hence, HHG seeding strongly favors ultrafast time-resolved

pump-probe applications; instead, a cascaded option is more suitable for those applications that demand high spectral brightness.

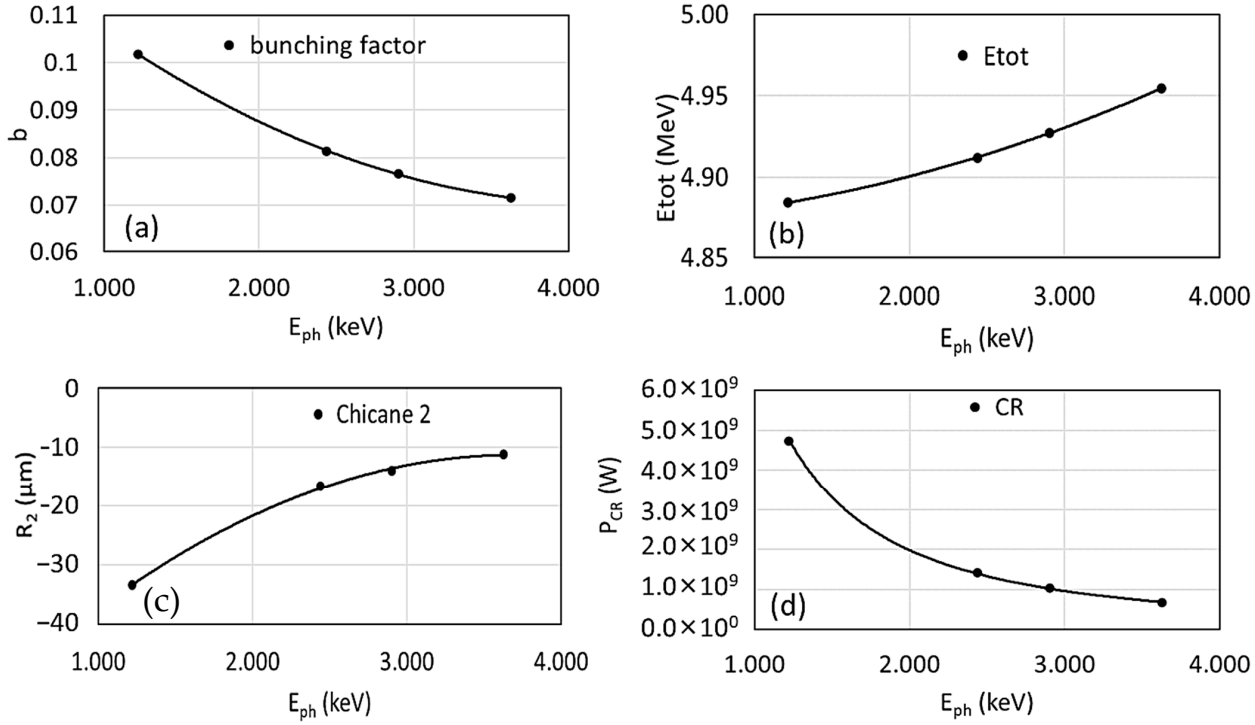

Figure 4. (**a**) In the HHG seeded EEHG option, the optimal bunching factor is shown as a function of photon energy. (**b**) The final energy spread (MeV) is shown as a function of photon energy (keV). (**c**) The momentum compaction of chicane 2 is shown as a function of photon energy. (**d**) The CR peak power is shown as a function of photon energy. Here, we assume the peak current is 300 A.

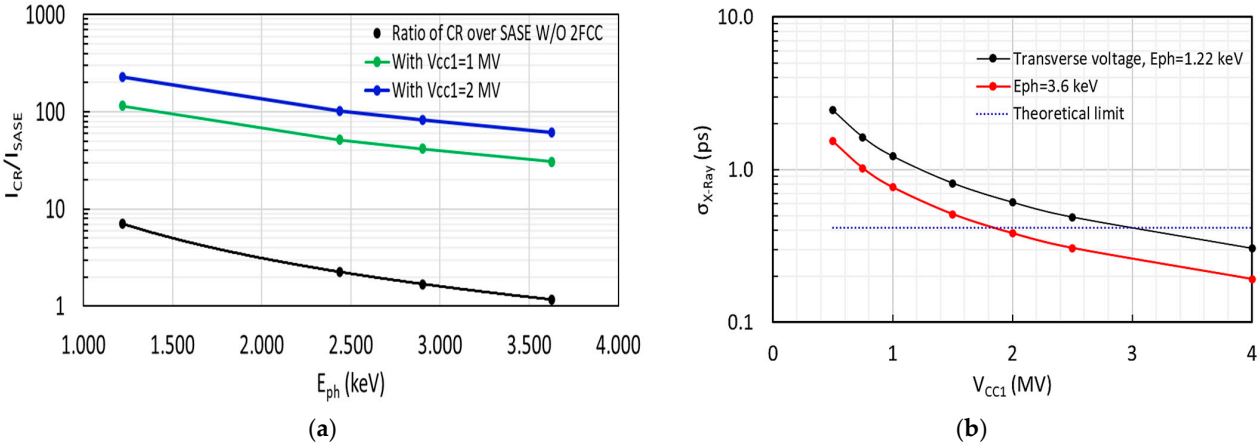

Figure 5. (**a**) In the HHG seeded EEHG option, the ratio of CR signal over SASE background (named SNR) is plotted as a function of photon energy in three cases: without 2FCC short-pulse scheme (black), with two-frequency crab cavity (2FCC) short-pulse scheme at $V_{CC1} = 1$ MV (green), and at $V_{CC1} = 2$ MV (blue). (**b**) Transverse voltage-limited pulse durations as a function of CC-1 voltage are plotted as the black ($E_{ph} = 1.22$ keV) and red ($E_{ph} = 3.6$ keV) curves, respectively; the shortest pulse estimated via Equation (9) is plotted as the blue dashed line.

2.2. SASE Background Removal via Two-Frequency Crab-Cavity Scheme

To fully benefit from the ultrashort (10 fs to 1 ps) coherent X-ray pulses generated with the EEHG scheme (Table 1), one must mitigate the SASE background, which is radiated by the entire electron bunch (e.g., 20 ps in RMS for the NSLS-II upgrade lattice) and contributes

not only as the noise to the detector, but also the unwanted exposure to the sample. The two-frequency crab cavity (2FCC) short-pulse scheme proposed by A. Zholents [36] could be an optimal solution to shorten the incoherent SASE radiation from 20 ps down to less than 1.1 ps depending on the radiation wavelength and maximum voltage of the crab cavity.

We apply a similar design implemented by X. Huang [37]. The two frequencies ($f_{1,2}$) of the crab cavities are 3 GHz ($f_1 = 6 \cdot f_{RF}$) and 3.25 GHz ($f_2 = 6.5 \cdot f_{RF}$), respectively. Here, the main RF frequency f_{RF} is 500 MHz for the NSLS-II upgrade. The crab cavities (CC) are operated at zero-crossing; thus, their main effects on the beam are to tilt the bunches vertically through the Z-dependent vertical kicks. A schematic of the three-cavity configuration is shown in Figure 6a [37]. For half of the buckets, the deflecting slopes of the two cavities would add up. Any bunch in those buckets acquires a steady-state vertical-longitudinal tilted equilibrium distribution; as it passes through a slit in the beamline, the bunch length would be shortened via such a Y–Z correlation, as shown in Figure 6b. For a complete cancellation of the deflecting slopes for the other half of the buckets, the center of the second CC must be well-aligned with the center of the straight section. The transverse voltage limited X-ray pulse length is estimated using Equation (8):

$$\sigma_{X-Ray}(V_{CC1}, \lambda_r) = \frac{E_0}{e_0 V_{CC1}} \frac{\sqrt{\frac{2\varepsilon_y}{L_u} + \frac{\lambda_r}{\pi L_u}}}{2\pi f_1} \left|\sin(\pi \nu_y)\right|. \quad (8)$$

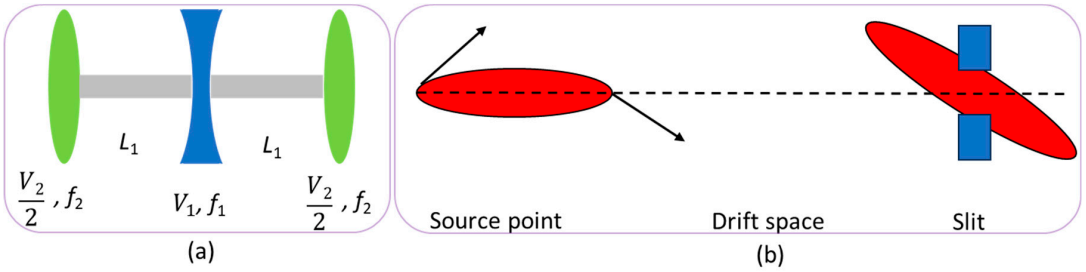

Figure 6. (**a**) Schematic of the three-cavity configuration for a complete cancellation [37]. (**b**) Propagation of photon beam from source point to slit in a drift space.

Here, V_{CC1} and V_{CC2} are the transverse voltages of crab cavity 1 and 2. V_{CC2} can be estimated by $V_{CC2} = V_{CC1}(1+u)$, where $u \approx \frac{e^{-\frac{1}{2}(a_1+a_2)^2(e^{2a_1a_2}-1)}}{1-e^{-2a_2^2}} - 1$. $a_1 = 2\pi f_1 \sigma_t$, $a_2 = 2\pi f_2 \sigma_t$, and $\sigma_t = 20$ ps (RMS electron bunch duration). V_{CC2} equals to $0.934 \cdot V_{CC1}$. Here, ε_y, λ_r, L_u, and ν_y are vertical emittance (e.g., 5 pm), radiation wavelength, radiator length (e.g., 3 m), and vertical tune (e.g., fraction 0.26), respectively. The shortest X-ray pulse, which can be achieved with this method in the limit of $\lambda_r/4\pi$, can be estimated via Equation (9) [37].

$$\dot{\sigma}_{X-Ray}(V_{CC1}, \lambda_r) = 2\sigma_t \left(\frac{T}{\tau_d} e^{-a_1^2} \cosh\left(a_1^2\right)\right)^{1/2} \left|\sin(\pi \nu_y)\right|. \quad (9)$$

Since the SASE background is the worst in the HHG seeded EEHG case, an ultrashort CR pulse with a few femtoseconds' duration could benefit most from the application of this 2FCC short-pulse scheme. We only consider the upper $\lambda_{r,max} = 1.02$ nm (E_{ph} = 1.22 keV) and lower $\lambda_{r,min} = 0.34$ nm (E_{ph} = 3.6 keV) bounds of the HHG seeded EEHG. Their transverse voltage limited pulse durations as a function of CC-1 voltage are plotted in Figure 5b as the black and red curves, respectively; the shortest pulse estimated via Equation (9) is plotted as the blue dashed line. As a result of applying the 2FCC short-pulse scheme, there is a factor of 16 up to 52 enhancement for the SNR, as shown in Figure 5a, depending on the CC-1 voltage and radiation wavelength. In addition, the application of a narrow spectral bandwidth monochromator in the HHG-seeding EEHG beamline could further reduce the SASE background noise.

2.3. Other FEL Options for Large-Sized SR

Since our design of an SR-based FEL is applicable to almost any SLS, to make the design complete, we should take most of the current and future fourth-generation DL-SLSs into account. Those SLSs can be divided into two categories: medium (e.g., NSLS-II upgrade)- and large (e.g., PETRA-IV)-sized SRs, by the following criteria: the circumference $L_C < 1$ km, and the straight section (SS) length $L_{SS} < 10$ m for medium SR and $L_C > 1$ km and $L_{SS} > 10$ m for large SR. The main difference is the allowable radiator length, a few meters for medium-sized SR and tens of meters for large-sized SR. Due to the recent progress on X-ray optics with the reflectivity of Bragg mirrors greater than 99% [38], X-ray free electron laser oscillator (XFELO) could be a vital option especially when the undulator distance can be up to tens of meters in a large-sized SR. The nearly perfect Bragg mirrors in the tender-to-hard X-ray wavelengths with the reflectivity R > 99% and Darwin width as narrow as a few μrad can be made from single-crystal diamonds with different orientations [39–41]. In addition, the beryllium-based compound lenses, which provide the desired focus to form a stable X-ray cavity, are commercially available [38,42]. There exist two conventional X-ray cavity designs, a four-mirror-based bow-tie cavity and a six-mirror cavity. The four- and six-mirror cavities provide 10% and 20% spectral tunability [43], respectively. SR-based XFELO can offer the highest spectral brightness [44,45] since the spectral bandwidth is only limited by the X-ray optics, which is in the order of 10^{-7} for 10 keV photon energy. Alternatively, SASE can be implemented for a large-sized SR. The advantage of SASE is that the initial energy spread can be kept to the minimum since SASE starts from the noise (no energy modulation). The long undulator length allows exponential growth; in conjunction with tapering, SASE can provide the highest photon flux compared to EEHG and XFELO.

Among those three cases, whereas there is a space limitation, prebunching should be the optimal choice; if there is no space limitation, besides EEHG, either SASE or XFELO can also be applied depending on the user-driven experimental preferences. SASE can provide the highest photon flux, whereas XFELO offers the narrowest spectral bandwidth as well as the highest spectral brightness. With the photon energy of 10 keV, characteristic comparison of SR-based FEL options of prebunching, SASE, and XFELO for medium-sized and large-sized storage rings are shown in Table 2. Moreover, thanks to the removal of space limitation, self-seeding could become a vital option. To make a comprehensive list of FEL options for the large SR case, we plan to explore a self-seeding option in our future studies.

Table 2. Characteristic comparison of SR-based FEL options of prebunching, SASE, and XFELO for medium and large sized SRs.

FEL Option at E_{ph} = 10 keV	**Prebunch (Cascaded EEHG)**	**SASE**	**XFELO**
Ring Size	Medium-SR	Large-SR	Large-SR
Photon energy range (keV)	0.1–10	0.1–10	10
Peak Power (MW)	170	100–300	0.1–1
Average Power (mW)	0.1–3	up to 1000	<10
Spectral Bandwidth (eV)	0.01–5	~7–17	0.003–0.01
Pulse Duration in RMS (ps)	0.01–1	>1	>1
Stability	Excellent	Poor	Excellent
Longitudinal Coherence	Good	Poor	Excellent
Transverse Mode	Defined by Electron Beam Size	Defined by Gain Guiding	Defined by Optical Cavity

Medium-SR with circumference < 1 km and straight section < 10 m. Large-SR with circumference > 1 km and straight section length > 10 m.

3. Method

We aim to provide design guidance for SR-based FELs, including medium- and large-sized SRs. To expand the capabilities of the NSLS-II upgrade and a potential future DL-SLS in the PEP tunnel [35], we consider a few FEL options using a low-emittance electron beam of NSLS-II upgrade and SDLS, which are synergetic with storage ring operations. The EEHG seeding option has been demonstrated with the capability of generating very narrow bandwidths and extremely high-brightness coherent EUV to soft X-ray pulses [1–9]. The focus of this manuscript is on the prebunching EEHG scheme using an EUV-HHG source to produce short pulses with photon energies ranging from tender and possible hard X-rays. Special care must be paid to mitigate the ISR and coherent synchrotron radiation (CSR) effects. The most severe ISR effect can be mitigated by optimizing the two-stage separation, and this has been summarized in our earlier study [13]. Regarding fourth-generation SLSs, momentum compactions are significantly smaller. To cover this range of X-rays, we chose the seed-laser wavelength of 256 nm for the first EEHG stage and an EUV-HHG source for the second stage. In addition, by varying the HHG pump laser wavelength (e.g., Yb 1030 nm and Ti:sapphire 800 nm) and gas type (Xenon, Krypton, and Argon) [10–12,26], the long wavelength limit can be extended up to >1 nm, overlapping with single-beamline EEHG (see Table 1). This design complements EEHG seeding using two optical seed lasers to cover the range from EUV to soft X-rays. Furthermore, by switching between a 256 nm conventional laser and the HHG source in the first stage for seeding only in cases when the HHG source has an adequate power in the near future, one can gain extra flexibility in manipulating the mini-energy stripe formation with the minimum energy modulation and least two-stage separation, thus mitigating the ISR effect, which is proportional to the two-stage separation and the effective energy heating effect due to the modulation only covering a few-femtosecond portion of the electron bunch overlapping for both stages.

4. Conclusions

With the availability of high-performing EUV-HHG seeding sources, we propose a novel HHG seeding EEHG option. It has been numerically demonstrated with the capability of generating coherent pulses with the tender X-ray spectrum [4–9,46–49]. The performances of the cascaded and HHG seeding options are quite similar, except that the HHG seeding generates the CR pulse in the level of a few femtoseconds, which is limited by the HHG seed pulse duration, instead being a few picoseconds in the cascaded case. HHG seeding could strongly benefit some special type of ultrafast time-resolved pump probe applications, including ultrafast science. Femtosecond—attosecond pulses can access ultrafast phenomena, e.g., electron dynamics, molecular vibrations, and energy transfer processes. X-ray probing together with synchronized optical laser pumping experiments enables an extremely high temporal resolution in the femtoseconds level. Instead, the cascaded option is more suitable for those applications that demand high spectrum brightness; see Table 1 for details. Furthermore, to fully benefit from HHG seeded EEHG, we apply a 2FCC short-pulse scheme to mitigate the SASE background noise; there is a factor of 16 up to 52 enhancement for SNR depending on the CC-1 voltage and radiation wavelength. It is worth noting that with the future advance on the HHG source, HHG seeding EEHG could potentially extend the shortest wavelength limit beyond the tender X-ray toward the hard X-ray spectrum.

Thanks to the removal of space limitation in the large sized SR case, we compared two cases with different undulator distances: one has the space limitation of a few meters, and the other can have the undulator distance of tens up to a hundred meters. In the first case with the space limitation, one can benefit significantly from the prebunching; instead, in the second case without space limitation, the FEL gain is dominated by the electron beam energy spread. One can also consider other options, e.g., SASE and XFELO. Among those cases, albeit there is a space limitation, prebunching should be the best choice; if there no space limitation, either SASE or XFELO can be applied beside EEHG, depending

on the user preferences, SASE can provide the high photon flux and XFEL could offer the narrowest spectral bandwidth.

Author Contributions: Conceptualization, investigation, and formal analysis, X.Y.; writing—original draft preparation, X.Y.; writing—review and editing, L.Y., V.S., and T.S.; funding acquisition, L.Y., V.S., and T.S. All authors have participated in the figure preparations. All authors have read and agreed to the published version of the manuscript.

Funding: This work was supported by Brookhaven National Laboratory Directed Research and Development Program. This manuscript has been authored by Brookhaven Science Associates under Contract No. DE-SC0012704 with the U.S. Department of Energy and Brookhaven National Laboratory LDRD 22-028. The United States Government retains and the publisher, by accepting the article for publication, acknowledges that the United States Government retains a non-exclusive, paid-up, irrevocable, worldwide license to publish or reproduce the published form of this manuscript, or allow others to do so, for United States Government purposes.

Data Availability Statement: The datasets generated and analyzed during the current study are not publicly available due to the reason that we want to know who has an interest in our datasets, but they are available from the corresponding author on reasonable request.

Acknowledgments: The authors are extremely grateful for the valuable discussion and great help from L. Giannessi.

Conflicts of Interest: The authors declare no competing financial and non-financial interests in relation to the work described in the paper.

References

1. Yang, X.; Penn, G.; Yu, L.H.; Smaluk, V.; Shaftan, T. Optimization of Echo-Enabled Harmonic Generation toward coherent EUV and soft X-ray free-electron laser at NSLS-II. *Sci. Rep.* **2022**, *12*, 9437. [CrossRef] [PubMed]
2. Yang, X.; Penn, G.; Smaluk, V.; Huang, X.; Yu, L.H.; Shaftan, T. Toward fully coherent soft X-ray free-electron laser via echo-enabled harmonic generation in 4th generation synchrotron light sources. *Rev. Sci. Instrum.* **2022**, *93*, 113101. [CrossRef] [PubMed]
3. Yang, X.; Penn, G.; Yu, L.H.; Huang, X.; Smaluk, V.; Shaftan, T. Twin-pulse seeding enables pump-probe capabilities in the EUV to soft X-ray spectrum at synchrotron light sources. *Sci. Rep.* **2023**, *13*, 5261. [CrossRef] [PubMed]
4. Bonifacio, R.; Pellegrini, C.; Narducci, L.M. Collective instabilities and high-gain regime in a free electron laser. *Opt. Commun.* **1984**, *50*, 373. [CrossRef]
5. Nuhn, H.D.; Tatchyn, R.; Winick, H.; Fisher, A.S.; Gallardo, J.C.; Pellegrini, C. Short wavelength FELs on large storage rings. *Nucl. Instrum. Methods A* **1992**, *319*, 89–96. [CrossRef]
6. Zhao, Z.T. Storage ring light sources. *Rev. Accel. Sci. Technol.* **2010**, *3*, 57. [CrossRef]
7. Mitri, S.D.; Cornacchia, M. Operating synchrotron light sources with a high gain free electron laser. *New J. Phys.* **2015**, *17*, 113006. [CrossRef]
8. Wang, X.; Feng, C.; Liu, T.; Zhang, Z.; Tsai, C.Y.; Wu, J.; Yang, C.; Zhao, Z. Angular dispersion enhanced prebunch for seeding ultrashort and coherent EUV and soft X-ray free-electron laser in storage rings. *J. Synchrotron Radiat.* **2019**, *26*, 677–684. [CrossRef] [PubMed]
9. Li, C.; Jiang, B.; Feng, C.; Huang, D.; Zhang, Q.; Wang, K. Lattice design for angular dispersion enhanced microbunching in storage rings. *J. Instrum.* **2021**, *16*, 03004. [CrossRef]
10. Zhang, X.; Lytle, A.L.; Popmintchev, T.; Zhou, X.; Kapteyn, H.C.; Murnane, M.M.; Cohen, O. Quasi-phase-matching and quantum-path control of high-harmonic generation using counterpropagating light. *Nat. Phys.* **2007**, *3*, 270–275. [CrossRef]
11. Ding, C.; Xiong, W.; Fan, T.; Hickstein, D.D.; Popmintchev, T.; Zhang, X.; Walls, M.; Murnane, M.M.; Kapteyn, H.C. High flux coherent super-continuum soft X-ray source driven by a single-stage, 10mJ, Ti:sapphire amplifier-pumped OPA. *Opt. Express* **2014**, *22*, 6194. [CrossRef] [PubMed]
12. Saule, T.; Heinrich, S.; Schötz, J.; Lilienfein, N.; Högner, M.; DeVries, O.; Plötner, M.; Weitenberg, J.; Esser, D.; Schulte, J.; et al. High-flux ultrafast extreme-ultraviolet photoemission spectroscopy at 18.4 MHz pulse repetition rate. *Nat. Commun.* **2019**, *10*, 458. [CrossRef] [PubMed]
13. Yang, X.; Yu, L.H.; Smaluk, V.; Shaftan, T.; Huang, X. Toward a fully coherent tender and hard X-ray free-electron laser via cascaded EEHG in fourth-generation synchrotron light sources. *J. Synchrotron Radiat.* **2023**, *30*, 861–875. [CrossRef] [PubMed]
14. Penco, G.; Perosa, G.; Allaria, E.; Badano, L.; Bencivenga, F.; Brynes, A.; Callegari, C.; Capotondi, F.; Caretta, A.; Cinquegrana, P.; et al. Nonlinear harmonics of a seeded free-electron laser as a coherent and ultrafast probe to investigate matter at the water window and beyond. *Phys. Rev. A* **2022**, *105*, 053524. [CrossRef]
15. Feng, C.; Zhao, Z. A Storage Ring Based Free-Electron Laser for Generating Ultrashort Coherent EUV and X-ray Radiation. *Sci. Rep.* **2017**, *7*, 4724. [CrossRef] [PubMed]

16. Feng, C.; Deng, H.; Zhang, M.; Wang, X.; Chen, S.; Liu, T.; Zhou, K.; Gu, D.; Wang, Z.; Jiang, Z.; et al. Coherent extreme ultraviolet free-electron laser with echo-enabled harmonic generation. *Phys. Rev. Accel. Beams* **2019**, *22*, 050703. [CrossRef]
17. Stupakov, G. Using the Beam-Echo Effect for Generation of Short-Wavelength Radiation. *Phys. Rev. Lett.* **2009**, *102*, 074801. [CrossRef] [PubMed]
18. Xiang, D.; Stupakov, G. Echo-enabled harmonic generation free electron laser. *Phys. Rev. Spec. Top.-Accel. Beams* **2009**, *12*, 030702. [CrossRef]
19. Molo, R.; Bakr, M.; Höner, M.; Huck, H.; Khan, S.; Nowaczyk, A.; Schick, A.; Ungelenk, P.; Zeinalzadeh, M. Echo-enabled harmonic generation at delta. In Proceedings of the IPAC2011, San Sebastián, Spain, 4–9 September 2011; p. 3074.
20. Evain, C.; Loulergue, A.; Nadji, A.; Filhol, J.M.; Couprie, M.E.; Zholents, A.A. Soft X-ray femtosecond coherent undulator radiation in a storage ring. *New J. Phys.* **2012**, *14*, 023003. [CrossRef]
21. Khan, S.; Bahnsen, F.; Cramm, S.; Döring, S.; Grewe, J.; Höner, M.; Huck, H.; Huck, M.; Molo, R.; Plucinski, L.; et al. Generation of Ultrashort and Coherent Synchrotron Radiation Pulses at DELTA. *Synchrotron Radiat. News* **2013**, *26*, 25–29. [CrossRef]
22. Khan, S. Ultrashort high-brightness pulses from storage rings. *Nucl. Instrum. Methods A* **2017**, *865*, 95. [CrossRef]
23. Willmott, P. *An Introduction to Synchrotron Radiation: Techniques and Applications*, 2nd ed.; Wiley: Hoboken, NJ, USA, 2019; ISBN-10 1119280397.
24. Xie, M. Design optimization for an X-ray free electron laser driven by SLAC linac. In Proceedings of the LINAC 1995 Particle Accelerator Conference, Dallas, TX, USA, 1–5 May 1995.
25. Giannessi, L. *Seeding and Harmonic Generation in Free-Electron Lasers, Synchrotron Light Sources and Free-Electron Lasers*; Springer International Publishing: Cham, Switzerland, 2015.
26. XUUS—High Harmonic Generation Source for EUV and Soft X-ray in KMLabs Inc. Available online: https://www.kmlabs.com/product/xuus (accessed on 1 November 2023).
27. Yu, L.H. Generation of intense UV radiation by subharmonically seeded single-pass free-electron lasers. *Phys. Rev. A* **1991**, *44*, 5178. [CrossRef] [PubMed]
28. Yu, L.H.; Ben-Zvi, I. High-gain harmonic generation of soft x-rays with the "fresh bunch" technique. *Nucl. Instrum. Methods Phys. Res. Sect. A* **1997**, *393*, 96. [CrossRef]
29. Yu, L.H.; Babzien, M.; Ben-Zvi, I.; DiMauro, L.F.; Doyuran, A.; Graves, W.; Johnson, E.; Krinsky, S.; Malone, R.; Pogorelsky, I.; et al. High-Gain Harmonic-Generation Free-Electron Laser. *Science* **2000**, *289*, 932–934. [CrossRef] [PubMed]
30. Yu, L.H.; Shaftan, T. Towards coherent X-ray free-electron lasers. *Nat. Photonics* **2019**, *13*, 513–515. [CrossRef]
31. Khan, S.; Büsing, B.; Held, A.; Mai, C.; Krishnan, A.R.; Salah, W.; Vijayan, V.; Usfoo, Z. SPEED: Worldwide first EEHG implementation at a storage ring. In Proceedings of the 14th International Particle Accelerator Conference (IPAC'23), Paper MOPM032. Venice, Italy, 7–12 May 2023. [CrossRef]
32. Ackermann, S.; Azima, A.; Bajt, S.; Bödewadt, J.; Curbis, F.; Dachraoui, H.; Delsim-Hashemi, H.; Drescher, M.; Düsterer, S.; Faatz, B.; et al. Generation of Coherent 19- and 38-nm Radiation at a Free-Electron Laser Directly Seeded at 38 nm. *Phys. Rev. Lett.* **2013**, *111*, 114801. [CrossRef]
33. Maltezopoulos, T.; Mittenzwey, M.; Azima, A.; Bödewadt, J.; Dachraoui, H.; Rehders, M.; Lechner, C.; Schulz, M.; Wieland, M.; Laarmann, T.; et al. A high-harmonic generation source for seeding a free-electron laser at 38 nm. *Appl. Phys. B* **2014**, *115*, 45–54. [CrossRef]
34. Schroer, C.G.; Roehlsberger, R.; Weckert, E.; Wanzenberg, R.; Agapov, I.; Brinkmann, R.; Leemans, W. *PETRA IV Conceptual Design Report*; DESY: Hamburg, Germany, 2019. [CrossRef]
35. Raimondi, P.; Huang, X.; Kim, J.; Safranek, J.; Rabedeau, T. Advanced storage ring lattice options based on hybrid six-bend achromat for Stanford Synchrotron Radiation Lightsource upgrade. *Phys. Rev. Accel. Beams* **2023**, *1061*, 169137. [CrossRef]
36. Zholents, A. A new possibility for production of subpicosecond X-ray pulses using a time dependent radio frequency orbit deflection. *Nucl. Instrum. Methods Phys. Res. Sect. A* **2015**, *798*, 111. [CrossRef]
37. Huang, X.; Hettel, B.; Rabedeau, T.; Safranek, J.; Sebek, J.; Tian, K.; Wootton, K.P.; Zholents, A. Beam dynamics issues for the two-frequency crab cavity short pulse scheme. *Phys. Rev. Accel. Beams* **2019**, *22*, 090703. [CrossRef]
38. Margraf, R.; Robles, R.; Halavanau, A.; Krzywinski, J.; Li, K.; MacArthur, J.; Osaka, T.; Sakdinawat, A.; Sato, T.; Sun, Y.; et al. Low-loss Stable Storage of X-ray Free Electron Laser Pulses in a 14 m Rectangular Bragg Cavity. *Res. Sq.* 2023; *preprint*. [CrossRef]
39. Kim, K.; Shvyd'ko, Y.; Reiche, R. A proposal for an X-ray free-electron laser oscillator with an energy-recovery linac. *Phys. Rev. Lett.* **2008**, *100*, 244802. [CrossRef]
40. Kim, K.; Shvyd'ko, Y. Tunable optical cavity for an x-ray free-electron-laser oscillator. *Phys. Rev. Spec. Top.-Accel. Beams* **2009**, *12*, 030703. [CrossRef]
41. Shvyd'ko, Y. *X-ray Optics—High-Energy-Resolution Applications*; Springer: Berlin/Heidelberg, Germany, 2004; Volume 98.
42. Kolodziej, T.; Stoupin, S.; Grizolii, W.; Krzywinski, J.; Shi, X.; Kim, K.J.; Qian, J.; Assoufid, L.; Shvyd'ko, Y. Efficiency and coherence preservation studies of Be refractive lenses for XFELO application. *JSR* **2018**, *25*, 354. [CrossRef]
43. Shvyd'ko, Y.; Stoupin, S.; Blank, V.; Terentyev, S. Near-100% Bragg reflectivity of X-rays. *Nat. Photonics* **2011**, *5*, 539. [CrossRef]
44. Margraf, R.; Robles, R.; Halavanau, A.; Kryzywinski, J.; Li, K.; MacArthur, J.; Osaka, T.; Sakdinawat, A.; Sato, T.; Sun, Y.; et al. Low-loss stable storage of 1.2 Å X-ray pulses in a 14 m Bragg cavity. *Nat. Photonics* **2023**, *17*, 878–882. [CrossRef]
45. Allaria, E.; De Ninno, G. A step towards cavity-based X-ray free electron lasers. *Nat. Photonics* **2023**, *17*, 841–842. [CrossRef]

46. Li, C.; Feng, C.; Jiang, B. Extremely bright coherent synchrotron radiation production in a diffraction-limited storage ring using an angular dispersion-induced microbunching scheme. *Phys. Rev. Accel. Beams* **2020**, *23*, 110701. [CrossRef]
47. Wang, X.; Feng, C.; Tsai, C.-Y.; Zeng, L.; Zhao, Z. Obliquely incident laser and electron beam interaction in an undulator. *Phys. Rev. Accel. Beams* **2019**, *22*, 070701. [CrossRef]
48. Zholents, A.; Zolotorev, M. Attosecond X-ray pulses produced by ultra short transverse slicing via laser electron beam interaction. *New J. Phys.* **2008**, *10*, 025005. [CrossRef]
49. Xiang, D.; Wan, W. Generating ultrashort coherent soft X-ray radiation in storage rings using angular-modulated electron beams. *Phys. Rev. Lett.* **2010**, *104*, 084803. [CrossRef]